Phase Distortion in a Propulsive Laser Beam Due to Aero-Optical Phenomena

Marco A. S. Minucci*
Instituto de Estudos Avancados, C.T.A., Brazil
and
Leik N. Myrabo†
Rensselaer Polytechnic Institute, Troy, New York

The interaction between a propulsive laser beam and the flowfield after the shock wave, generated during the flight of a beam-powered conical-shaped transatmospheric vehicle, is studied. Although the adopted theoretical model is a simplified one, the results of this study anticipate some of the aero-optical phenomena to be expected during a beamed transatmospheric flight. By considering a propulsive beam operating at 3.8 μm, phase distortions up to 51.41 wavelengths are reported. The range of flight Mach numbers covered by the present analysis falls between 1.67 and 20. As a major conclusion, considerable beam degradation can be expected only during the beginning of the beamed transatmospheric flight.

Nomenclature

c = limiting velocity for adiabatic expansion into vacuum
D = propulsive laser beam diameter
L = optical path length
M = Mach number
n = index of refraction
P = optical phase distortion
p = pressure
r,α = polar coordinates in xy plane, with origin at tip of cone
S = distance measured along laser beam, with origin at intersection of incoming laser beam and xy plane
T = absolute temperature
U = velocity along conical ray
V = velocity normal to a conical ray
x,y,z = Cartesian coordinate axes, with origin at tip of cone (z = cone axis)
x',y' = Cartesian coordinate axes at incoming laser beam shadow xy plane, with origin at center of beam shadow
$r'\theta'$ = polar coordinates at incoming beam shadow in xy plane, with origin at center of beam shadow
γ = ratio of specific heats
θ = conical ray angle from cone axis
κ = Gladstone-Dale constant for infrared radiation
λ = wavelength
ρ = air density
τ = aero-optical coefficient

Subscripts

G = values in gap between TAV forebody surface and receiving optics
i,j = values at two arbitrary rays i and j inside the laserbeam
0 = a reference value
s = values at cone surface
SL = values at sea level
w = values at shock-wave surface
I = ERH and scramjet thruster modes
II = MHD-fanjet mode
∞ = freestream conditions

Superscript

* = quantity is divided by $(\kappa'/\lambda)(\rho_\infty/\rho_{SL})$

Introduction

THE idea of using a propulsive beam in reusable spacecraft for Earth-to-orbit missions is not new. It was first suggested by Willinski[1] in 1958. More recently, a successful flight of a microwave beam-powered aircraft[2] was reported. Besides that atmospheric flight, there are several research programs currently underway to develop a reusable beam-powered transatmospheric vehicle (TAV). The analysis in the present work deals with one of them, which is being carried out at Rensselaer Polytechnic Institute: the Apollo Lightcraft Project.[3] The laser-powered Apollo Lightcraft is an advanced vehicle designed to enable manned missions (up to five passengers plus cargo) to low Earth orbit, or even to the moon, with very low operational costs.

The Apollo Lightcraft will have to cross the Earth's atmosphere at supersonic and hypersonic velocities while receiving a very intense laser beam ($\sim 10^4$ W/cm^2). Before this beam can be taken into the propulsive engines, it must first traverse a conical shock wave caused by an external compression inlet across the vehicle forebody. As is well-known, a compressible flow over a laser mirror or window causes variations in air density and the index of refraction. These variations introduce a phase shift (or distortion) in the beam. This phase distortion creates optical aberrations in the propulsive beam such as tilting, refocusing, astigmatism, and coma. The intensity of these aberrations can be evaluated using the Zernike polynomial coefficients, but they will not be calculated in this work.

For the sake of simplicity, a few simplifying assumptions are introduced:

1) The Apollo Lightcraft forebody is assumed to be conical.
2) During the flight, the vehicle angle of attack is set equal to zero.
3) The flow over the mirror (or windows) is assumed to be inviscid.
4) The air behaves as an ideal gas.

Presented as Paper 88-2972 at the AIAA/ASME/SAE/ASEE 24th Joint Propulsion Conference, Boston, MA, July 11-13, 1988; received Dec. 30, 1988; revision received May 30, 1989.

*Graduate Student, Rensselaer Polytechnic Institute. Member AIAA.
†Assistant Professor. Member AIAA.

5) The shock wave is regarded as a discontinuity surface of zero thickness.

The impact of these assumptions on the phase-distortion calculations is discussed below.

The work reported here is based on a previous investigation accomplished by A.E. Fuhs and S.E. Fuhs on laser turrets.[4] Therefore, the notation adopted in this paper (with regard to phase-distortion calculations) will be the same as that of Ref. 4.

Background Information About the Apollo Lightcraft

In this section, some features of the Apollo Lightcraft concept that are relevant for the following sections are presented. For more details, the interested reader is advised to consult Refs. 3 and 6.

Figure 1 is a sketch of the 2.5 GWe Apollo-sized orbital shuttlecraft that would use advanced combined-cycle engines for propulsion. As indicated in Fig. 1, beam power is first received by the Apollo Lightcraft across a 4.25-m-diam centerbody primary optics. The laser power will be provided by space-based free electron lasers (FEL) having efficiencies of at least 25% and will probably be available by 2020 if current SDI support continues. The electric power levels required to operate the lasers will be achieved through the use of 10 GWe Satellite Solar Power Stations,[3] probably available sometime in the early 21st century. By the use of low-Earth orbital relay satellites, the laser power is redirected to the spacecraft. Twelve cylindrical laser beams equally spaced along the primary optics circumference deliver the propulsive power to the TAV. Because of symmetry, only one beam-shock wave interaction needs to be studied.

While accelerating to orbit, the Apollo Lightcraft combined-cycle engine would "shift gears" three times. The advanced engine would have three air-breathing modes, plus a rocket mode for orbit circularization. The combined-cycle engine is as follows: mode 1: ERH thruster, mode 2: scramjet, mode 3: magnetohydrodynamic (MHD)-fanjet, and mode 4: laser-heated rocket. All engine modes are powered by beamed energy.

The external radiation heated (ERH) thruster is an airbreathing pulsejet engine which utilizes a high-intensity repetitively-pulsed laser beam to produce thrust. This process is

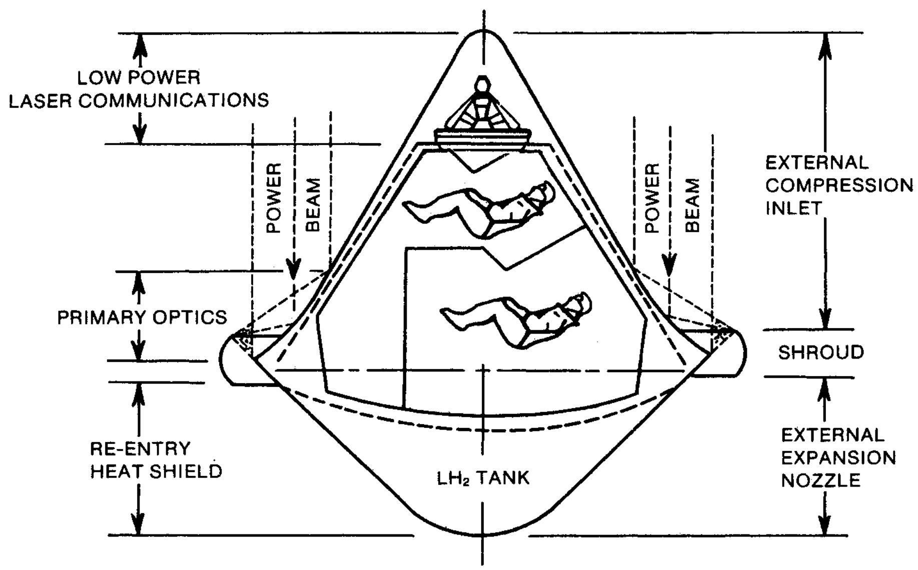

Fig. 1 Apollo Lightcraft configuration (2.4 *GWe* beam power).

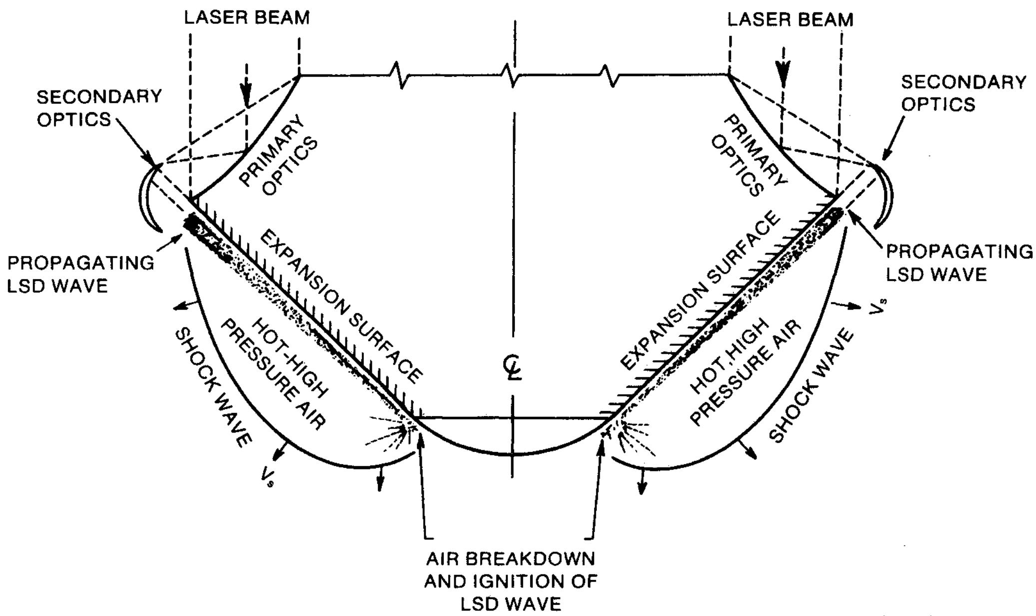

Fig. 2 Apollo Lightcraft in ERH thruster mode.

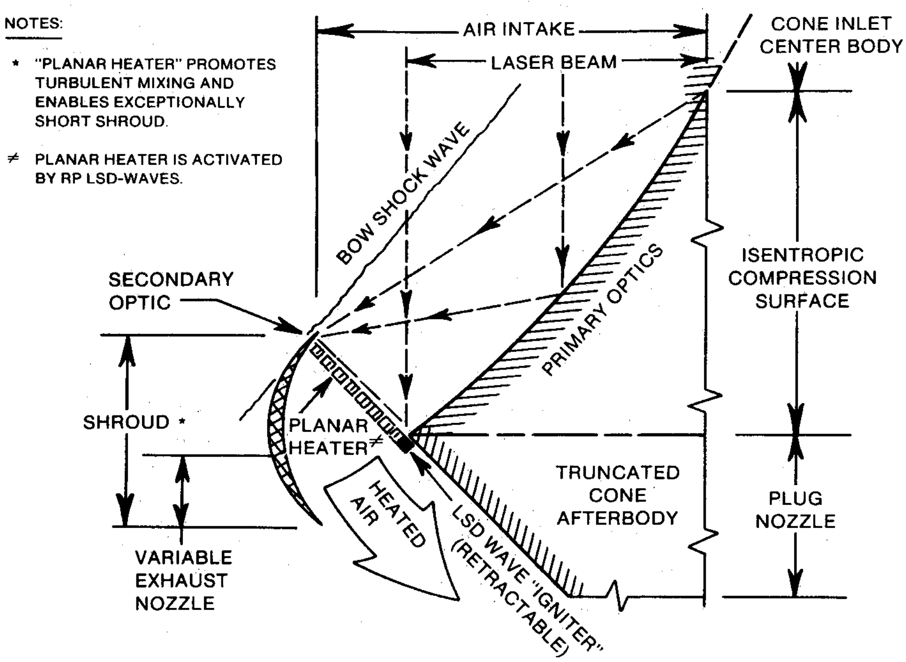

Fig. 3 Apollo Lightcraft in scramjet mode.

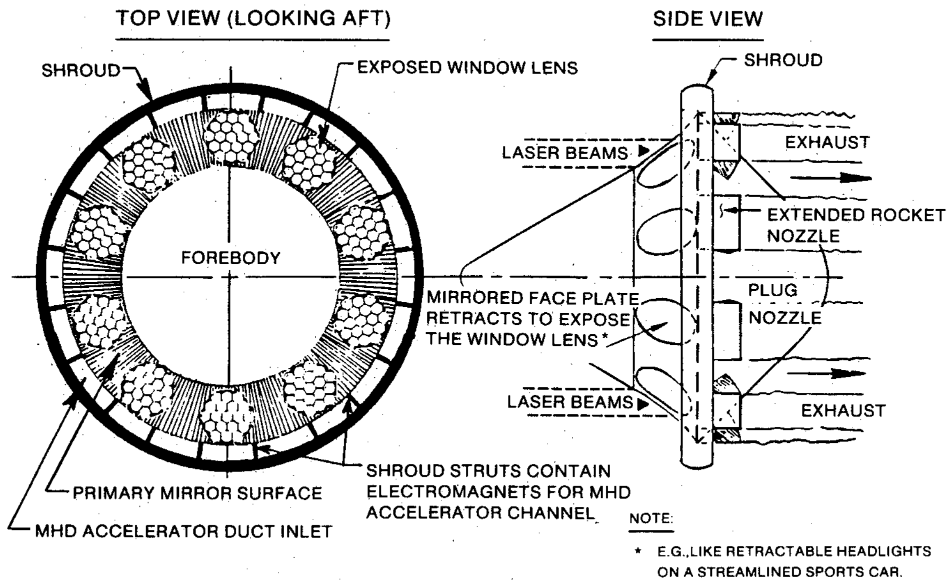

Fig. 4 Apollo Lightcraft in MHD-fanjet or rocket mode.

accomplished by a series of laser-induced cylindrical blast waves, which are initiated adjacent to the Apollo aft centerbody (thruster surface); as these blast waves expand, an impulse is delivered to this surface. Figure 2 portrays the Apollo Lightcraft in the ERH thruster mode, which is used for powered vertical takeoffs and landings, as well as accelerations up to Mach 3 and 20,000 ft. Upon reaching Mach 3, propulsive power would be transferred to the scramjet mode. This first shift is necessary because the net thrust of the ERH engine decreases more rapidly with increasing altitude and Mach number than the scramjet does. Although both propulsive cycles involve laser heating of the air, the ERH thruster depends more heavily on the laser pulse repetition rate (PRF). In the ERH thruster mode, PRF must be decreased with increasing altitude because more time is needed (between laser pulses) to completely expand the hot, high-pressure air (Fig. 2). This "expansion time" is increased due to the low static pressures found at higher altitudes.[3]

In the scramjet mode, the incoming laser power would be absorbed within the annular shroud region. An annular "planar heater" (pictured in Fig. 3) would be created by repetitively pulsed LSD waves that propagate at right angles across the duct flow,[3,6] This "planar heater" adds enthalpy to the supersonic duct flow much in the manner of current scramjets which rely on chemical fuels.

At some point beyond Mach 10, frozen flow losses would dominate, and thrust would fall to zero. The Apollo Lightcraft engine would then transition to the MHD-fanjet propulsion cycle portrayed in Fig. 4. In this mode, laser-heated H_2 rocket gas MHD generators would extract electrical power and deliver it to an air-breathing "electric fan," which uses MHD forces to accelerate the air. The blunt conical forebody will promote ionization at the lowest possible flight Mach numbers, at the cost of producing a strong blow shock.

Because of the wide Mach number range flown by the Apollo Lightcraft, the annular shroud (depicted in Figs. 1–4) will translate aft to keep the conical bow shock attached at the shroud forward lip. To survive the severe aeroheating anticipated at hypersonic Mach numbers, the primary optics mirror surface (forebody) and the shroud must regeneratively cooled; the liquid hydrogen expendables used in the last two propulsion modes serve as the heat sink.

From the above, it is observed that the performance of the Apollo Lightcraft strongly depends on the laser beam "quality." Furthermore, in the first two thruster modes (ERH and scramjet), the focus position at the secondary optics (shroud) is critical. A slight movement of that focus can drastically alter the TAV trajectory.[3] Even for the last two thruster modes (MHD-fanjet and rocket), if the beam degradation is too high, the impulse coupling coefficient will decrease. As a consequence the global efficiency of the system will also decrease.

Because beam degradation can be predicted by knowing the optical phase-distortion distribution over the beam wavefront,[5,7] the present analysis is fully justified.

Apollo Lightcraft Simplified Forebody

In order to evaluate the beam degradation due to aero-optical phenomena, some simplifications will be introduced. The isentropic, spike-shaped Apollo forebody will be replaced by a conical approximation. This geometry will retain the same original 30-deg semiapex angle but will not have the subsequent parabolic section. With this assumption, airflow over the forebody will be conical. Therefore, the computed density gradients will be lower than the real ones. This occurs since the simplified flow does not take into account the additional compression introduced by the downstream parabolic section. As will be seen, the optical phase distortion is proportional to the density gradients crossed by the beam. Hence, the predicted values for beam distortion will be lower than the actual ones.

Another implication of the previous assumption is that the primary optics used in this investigation will be conical. As a result there will be no focusing effect in this analysis.

The Apollo Lightcraft simplified forebody indicated with one of the 12 propulsive laser beams is shown in Figs. 5 and 6. Figure 5 portrays a simplified version of the ERH and scramjet thruster modes, whereas Fig. 6 depicts the simplified situation for the MHD-fanjet mode.

In both the ERH and scramjet thrust modes, it is of interest to evaluate the optical phase distortion at the primary optics focus point. In the simplified geometry depicted in Fig. 5, the problem is approximately equivalent to computing the phase distortion when the reflected beam emerges from the conical wave.

On the other hand, in the MHD-fanjet mode the goal is to calculate the phase-distortion distributions dveloped by the beam at the receiving optics—*inside* the TAV (as seen in Fig. 6).

Both Figs. 5 and 6 show a cross section of the vehicle and one of the 12 cylindrical beams in the xy plane. This plane contains both the TAV axis and the laser-beam axis. Note that θ_s stands for the cone semiapex angle, r_o is the distance between the TAV centerline and the laser-beam axis, r_i is the distance between a generic ray "i" inside the beam and the TAV axis, D is the beam diameter, θ is the polar coordinate, and S is a distance along the laser beam. The cylindrical coordinates α and r determine a specific starting ray inside the beam. Finally, M_∞ is the freestream or flight Mach number.

Laser-Beam Phase-Distortion Calculations

Although the optical phase distortion can be caused by an external viscous flowfield,[4,8] the following calculations will not take into account such viscous flow phenomena. The

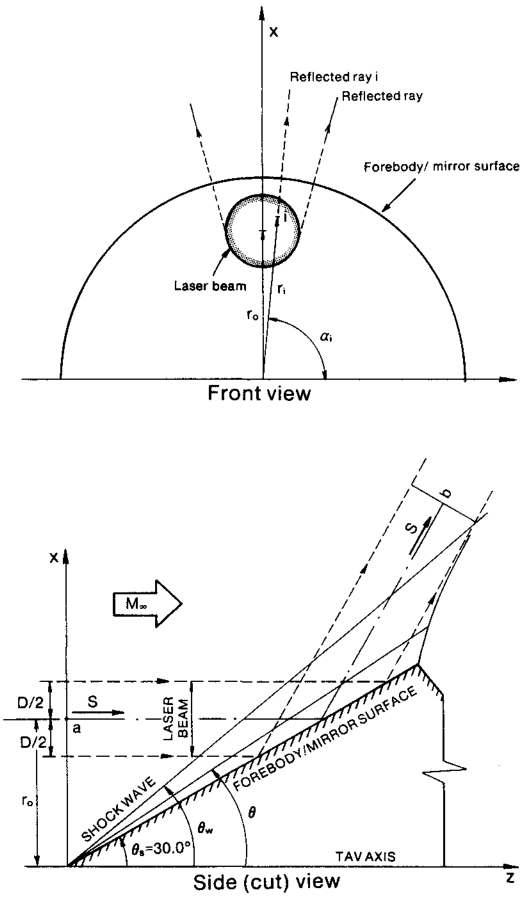

Fig. 5 Simplified concial geometry for the Apollo Lightcraft forebody in ERH or scramjet thruster mode. Neither the shroud nor the plug nozzle were represented.

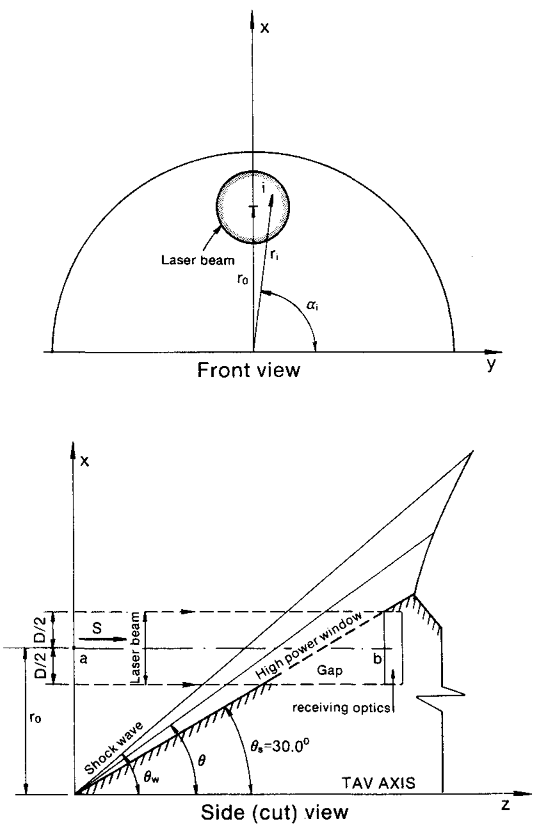

Fig. 6 Simplified geometry for the Apollo Lightcraft forebody in MHD-fanjet mode. Neither the shroud nor the plug nozzle were represented.

conical flowfield will be assumed to be inviscid. Therefore, only the optical phase distortion due to an external inviscid flowfield will be considered in this work.

The phase-distortion problem is not restricted to beamed transatmospheric flight; very similar problems occur in gasdynamic[9] and chemical lasers (i.e., flow lasers in general), aerodynamic windows,[9,10] and laser turrets.[4] In all of these cases, an optical phase distortion is developed by a laser beam due to density inhomogeneities in the propagation and/or generation media.

The optical phase distortion P can be defined as the difference in the optical path length ΔL between two rays i and j within the laser beam divided by the wavelength of the radiation. So,

$$P_{ji} = \frac{\Delta}{\lambda} = \frac{L_j - L_i}{\lambda} \tag{1}$$

On the other hand, the optical path length L_i for a particular ray i inside the laser beam is defined as

$$L_i = \int_a^b n(S_i)\mathrm{d}S \tag{2}$$

where S is the distance along ray i and the points a and b are positioned, respectively, in the undisturbed (incoming) and disturbed (outcoming) laser-beam wavefronts (Figs. 5 and 6). The index of refraction n is a function of S. As a consequence, Eq. (2) can be written as

$$P_{ji} = \frac{1}{\lambda}\int_a^b [n(S_j) - n(S_i)]\ \mathrm{d}S \tag{3}$$

The local index of refraction n is related to the local gas density ρ by

$$n = 1 + \kappa\frac{\rho}{\rho_\infty} = 1 + \kappa'\left(\frac{\rho_\infty}{\rho_{SL}}\right)\left(\frac{\rho}{\rho_\infty}\right) \tag{4}$$

where ρ_∞ is the freestream density at the TAV altitude, and ρ_{SL} is the density at sea level. The constant κ' has a value of approximately 2.3×10^{-4} for infrared radiation. From Eqs. (3) and (4), one can obtain

$$P_{ji} = \frac{\kappa'}{\lambda}\frac{\rho_\infty}{\rho_{SL}}\int_a^b \left[\left(\frac{\rho}{\rho_\infty}\right)_j - \left(\frac{\rho}{\rho_\infty}\right)_i\right] \mathrm{d}S \tag{5}$$

The above expression shows a dependence on altitude through the term ρ_∞/ρ_{SL} and on the density ratio ρ/ρ_∞. The subscripts i and j in the density ratio terms refer to the density ratio along the rays i and j, respectively.

Conical Flowfield Solution

From Eq. (5) in the previous section, the calculation of the phase distortion requires the knowledge of the density ratio ρ/ρ_∞. This density ratio can be obtained by solving the Euler equation with suitable boundary conditions. These boundary conditions are the TAV forebody geometry and the shock wave. By assuming a conical forebody and isentropic flow behind the shock wave, one can write[11]:

$$\frac{\mathrm{d}U}{\mathrm{d}\theta} - V = 0 \tag{6}$$

$$\frac{\mathrm{d}V}{\mathrm{d}\theta} - U + \frac{1}{\rho V}\frac{\mathrm{d}p}{\mathrm{d}\theta} = 0 \tag{7}$$

$$\frac{\mathrm{d}(\rho V \sin\theta)}{\mathrm{d}\theta} + 2\rho U \sin\theta = 0 \tag{8}$$

with the following boundary conditions:

Wall condition at:

$$\theta = \theta_s \rightarrow U = U_s \text{ and } V = 0$$

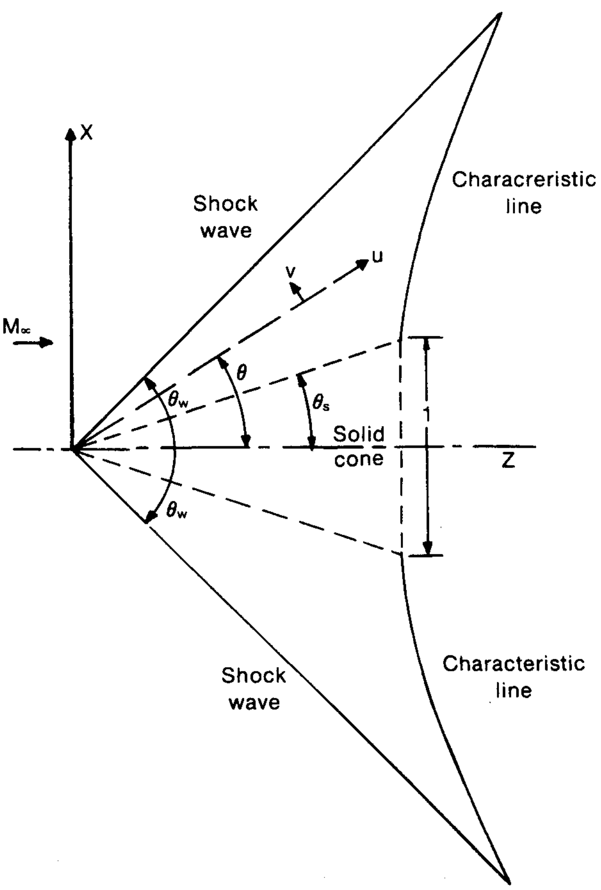

Fig. 7 Polar coordinate system of conical shock.

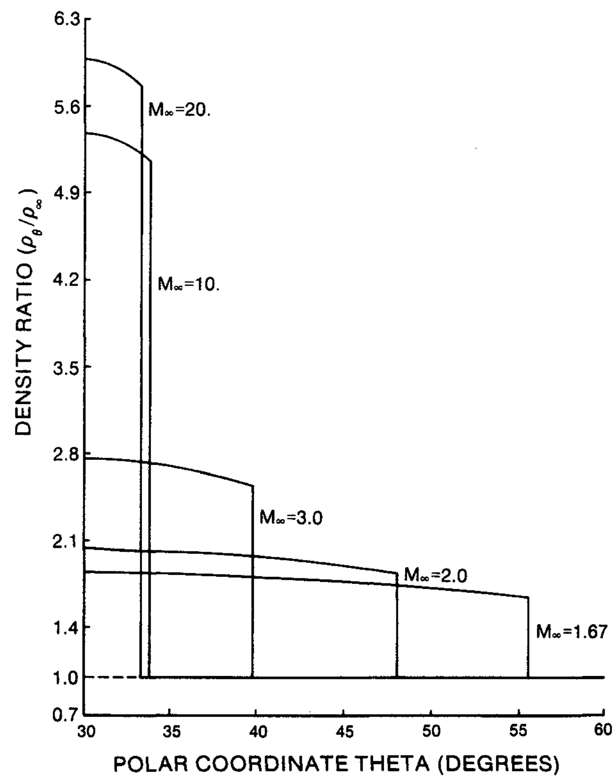

Fig. 8 Density ratio vs θ and M_∞.

Shock conditions at

$$\theta = \theta_s \rightarrow U = U_w \text{ and } V = V_w$$

where θ_w, U_w, and V_w must satisfy the following relations:

$$\tan\theta_w = \frac{\gamma - 1}{\gamma + 1}\,\frac{c^2 - U_w^2}{U_w V_w} \tag{9}$$

$$M_\infty = \left(\frac{2}{\gamma - 1}\right)\frac{U_w^2}{c^2\cos^2\theta_w - U_w^2} \tag{10}$$

$$c^2 = U_\infty^2\left[1 + \frac{2}{\gamma - 1}M_\infty\right] \tag{11}$$

where γ is the ratio of specific heats, U and V are the flowfield velocity components in the polar coordinate system, ρ is the local density, p is the local pressure, and c is the velocity the fluid would obtain if allowed to expand adiabatically into a vacuum. All of the presented variables are shown in Fig. 7.

Equations (6-8) must be solved numerically subject to the boundary conditions indicated above. This task was first accomplished by Kopal[12] and later by Sims.[13] These equations indicate that the flow properties ρ, p, and T (absolute temperature) can be written in terms of the polar coordinate θ; thus, the flow properties are constant over imaginary conical surface located between the conical shock wave and the TAV surface. Figure 8 shows the density ratio $\rho(\theta)/\rho_\infty$ as a function of θ for several flight Mach numbers.

Note that all plots involving the flight Mach number M_∞ start at $M_\infty = 1.67$, since this is the lowest M_∞ which provides an attached conical shock wave for $\theta_s = 30$ deg.

Numerical Results

From the preceding section, Eq. (5) can be written as

$$p_{ji} = \frac{\kappa'}{\lambda}\left(\frac{\rho_\infty}{\rho_{SL}}\right)\int_a^b\left\{\left[\frac{\rho(\theta)}{\rho_\infty}\right]_i\right\}\mathrm{d}S \tag{12}$$

If one assumes that a is located at the incident wavefront and b is located at the wavefront from which the phase distortion is to be evaluated, the optical phase distortion becomes

$$p_{ji} = \frac{\kappa'}{\lambda}\left(\frac{\rho_\infty}{\rho_{SL}}\right)\int_0^{s_O}\left\{\left[\frac{\rho(\theta)}{\rho_\infty}\right]_i\right\}\mathrm{d}S \tag{13}$$

where S_O is the distance between the two considerd wavefronts, measured along the laser-beam axis.

After some geometrical reasoning, one obtains the following: For the ERH and scramjet thruster modes,

$$p_{ji} = \frac{\kappa'}{\lambda}\frac{\rho_\infty}{\rho_{SL}}(r_j - r_i)\left\{\frac{1}{\tan\theta_w} - \int_{\theta_w}^{\theta_s}\left[\frac{\rho(\theta)}{\rho_\infty}\right]\frac{\mathrm{d}\theta}{\sin^2\theta}\right\}_i - \frac{1}{\tan(2\theta_s - \theta_w)} + \frac{\kappa'\rho_\infty}{\lambda\rho_{SL}}(r_j - r_j) \times\left\{\int_{\theta_w}^{\theta_s}\left[\frac{\rho(\theta)}{\rho_\infty}\right]\frac{\mathrm{d}\theta}{\sin^2(2\theta_s - \theta)}\right\} \tag{14}$$

And for the MHD-fanjet mode,

$$p_{IIji} = \frac{\kappa'\rho_\infty}{\lambda\rho_{SL}}(r_j - r_i)\left\{\frac{1}{\tan\theta_w} - \int_{\theta_w}^{\theta_s}\left[\frac{\rho(\theta)}{\rho_\infty}\right]\frac{\mathrm{d}\theta}{\sin^2\theta}\right\} - \frac{\kappa'\rho_\infty}{\lambda\rho_{SL}}(r_j - r_i)\left[\left(\frac{\rho_G}{\rho_\infty}\right)\frac{1}{\tan\theta_s}\right] \tag{15}$$

where r_i is the distance between ray i and the cone axis measured at the incident wavefront (plane xy in Figs. 5 ad 6) and ρ_G is a reference density, assumed equal to the density at the mirror surface. The use of this reference density comes from the existence of a gap between the receiving optics and the forebody surface. This gap is indicated in Fig. 6.

Note that the last factors in Eqs. (14) and (15) are functions of the flight Mach number, cone angle, and optical path only. Thus, it is possible to introduce the aero-optical coefficient τ defined by

$$\tau_I = \frac{1}{\tan_w} - \int_{\theta_w}^{\theta_s}\left[\frac{\rho(\theta)}{\rho_\infty}\right]\frac{\mathrm{d}\theta}{\sin^2\theta} + \int_{\theta_w}^{\theta_s}\left[\frac{\rho(\theta)}{\rho_\infty}\right]\frac{\mathrm{d}\theta}{\sin^2(2\theta_s - \theta)} - \frac{1}{\tan(2\theta_s - \theta_w)} \tag{16}$$

for the ERH and scramjet thruster modes; and by

$$\tau_{II} = \frac{1}{\tan\theta_w} - \int_{\theta_w}^{\theta_s}\left[\frac{\rho(\theta)}{\rho_\infty}\right]\frac{\mathrm{d}\theta}{\sin^2\theta} - \left(\frac{\rho_G}{\rho_\infty}\right)\frac{1}{\tan\theta_s} \tag{17}$$

for the MHD-fanjet mode. The aero-optical coefficient τ (introduced herein) actually measures the effect of the compressed flowfield upon the laser beam. In other words, this coefficient indicates how strong the "flow/laser beam" interaction is likely to be.

As an important result, Eqs. (14) and (15) can be rewritten as

$$P_{I,ji} = \frac{\kappa'}{\lambda}\frac{\rho_\infty}{\rho_{SL}}(r_j - r_i)\tau_I \tag{18}$$

$$P_{II,ji} = \frac{\kappa'}{\lambda}\frac{\rho_\infty}{\rho_{SL}}(r_j - r_i)\tau_{II} \tag{19}$$

The numerical calculation of τ_I and τ_{II} encompasses the numerical evaluation of the integrals in Eqs. (16) and (17).

As stated before, in all of the calculations, the shock wave itself was treated as a discontinuity surface with zero thickness. Consequently, the refraction of the beam as it passes

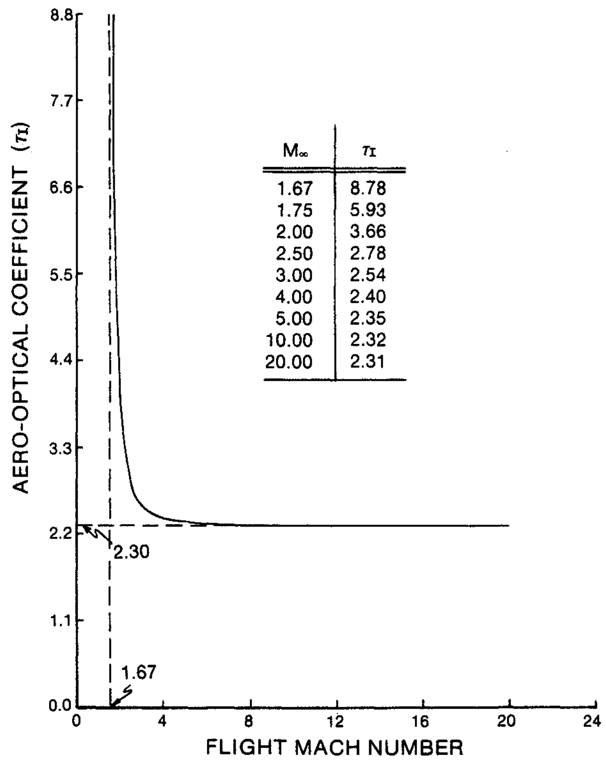

Fig. 9 Aero-optical coefficient vs flight Mach number in ERH or scramjet modes.

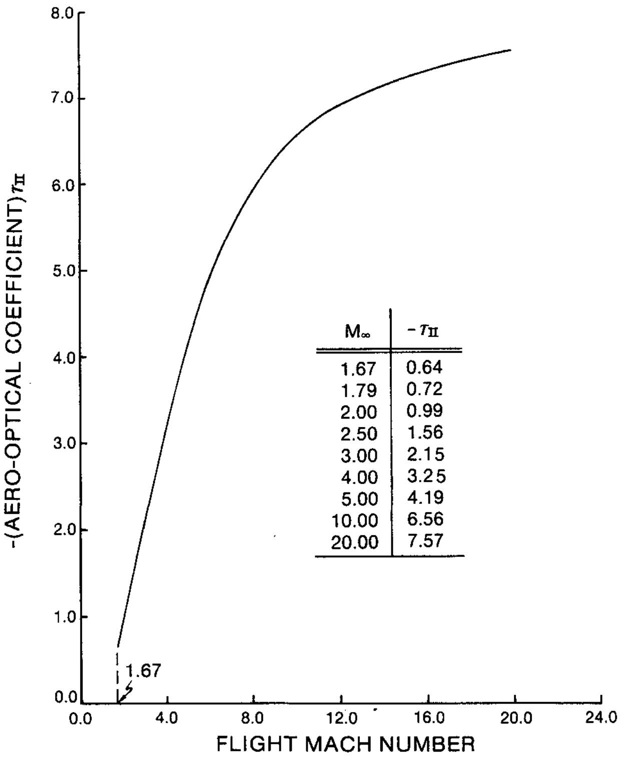

Fig. 10 Aero-optical coefficient vs flight Mach number in MHD-fanjet mode.

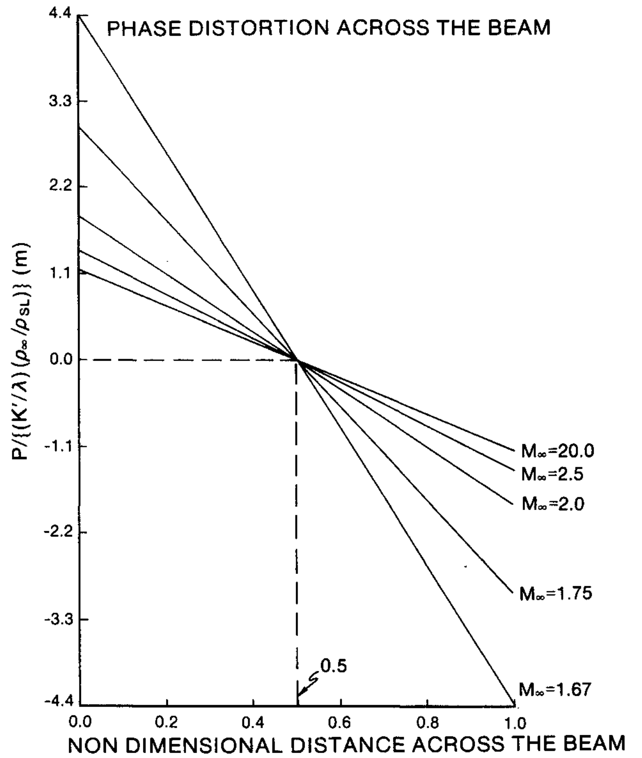

Fig. 11 Variation of P_I^* along a selected beam (evaluated just after the reflected beam has transversed the shock wave).

through the shock-wave region has been neglected. This hypothesis is entirely compatible with the ideal-gas assumption, and the first-order approximation goal for this work.

Figures 9 and 10 exhibit the variation of the defined aero-optical coefficients with flight Mach number. In Fig. 9 (the ERH/scramjet mode), one sees a tremendous drop of the aero-optical coefficient in the Mach range of 1.67–4.00. Beyond this point, τ_I remains approximately constant with increasing Mach numbers. This lower limit is indicated in Fig. 9.

On the other hand, Fig. 10 (the MHD-fanjet mode) portrays a different behavior for the aero-optical coefficient, when compared to the previous case. Now τ_{II} increases (in an absolute way) with increasing flight Mach number up to a certain limit—probably attained beyond Mach 24.

The opposite behavior of the aero-optical coefficient observed in Figs. 9 and 10 is associated with the different geometric constraints of the two cases. In the first case, the aero-optical coefficient τ_I is evaluated when the reflected beam crosses the shock wave. This means that τ_I is being evaluated after the laser beam has crossed the supersonic conical flow twice. As a consequence, the distortions introduced by the flow in the beam during its first passage are attenuated during the second passage (i.e., after the beam has been reflected by the mirror). The intensity of this attenuation, of course, is a function of the flight Mach number, which is introduced in Eq. (16) by the density ratio $\rho(\theta)/\rho_\infty$ and the conical shock angle θ_w.

In turn, the aero-optical coefficient τ_{II} is evaluated at the receiving optics inside the Apollo Lightcraft. As a result, the propulsive beam crosses the supersonic flow only once, and the optical aberrations introduced during that passage are not counteracted by a second passage.

Both the lower and upper limits—observed in Figs. 9 and 10, respectively—are due to the physical upper limit imposed on the density ratio and the shock angle θ_w as the flight Mach number M_∞ tends to infinity.

By choosing the ray starting at the laser-beam axis as a reference ray and dropping the subscripts i and j, Eqs. (18) and (19) can be written as

$$P_I = \frac{\kappa'}{\lambda}\frac{\rho_\infty}{\rho_{SL}}(r - r_0)\tau_I \tag{20}$$

$$P_{II} = \frac{\kappa'}{\lambda}\frac{\rho_\infty}{\rho_{SL}}(r - r_0)\tau_{II} \tag{21}$$

where $r(r_0 - D/2 < r < r_0 + D/2)$ represents the distance between a generic ray starting at $z=0$ and the beam axis, and r_0 is the distance between the incident beam axis at $z=0$ and the cone axis. In order to separate out the altitude and wavelength effects on the optical phase distortion, plots of P_I and P_{II} divided by the factor $(\kappa'/\lambda)(\rho_\infty/\rho_{SL})$ as a function of nondimensional distance across the beam diameter are portrayed in Figs. 11 and 12, respectively. Let P_I^* and P_{II}^* denote values of P_I and P_{II} divided by the factor indicated above. The chosen beam diameter is that defined by the interaction between the xy plane and the considered laser beam.

Equations (20) and (21) define the existence of constant phase-shift contours inside the beam. If P_{II}, ρ_∞/ρ_{SL}, and τ_{II} are held constant, one obtains

$$r - r_0 = \text{constant} \tag{22}$$

Equation (22) defines a family of concentric circumferences over the plane $z=0$ with their centers lying at the origin of x,y,z coordinate system (i.e., at the cone apex). Figure 13 shows some maps of constant P_{II} contours for three different flight Mach numbers assuming $D = 1.00$ m and $r_0 = 1.65$ m.

Similar results can be obtained for Eq. (20), but due to the conical reflection (as seen in Fig. 14), the constant P_I^* contours are difficult to represent.

Because the TAV is flying out through the atmosphere, altitude is always increasing causing the factor ρ_∞/ρ_{SL} to decrease. As a result, a complete evaluation of the phase-plane distortion requires a correlation between altitude and flight Mach number. This correlation is provided by a trajectory-al-

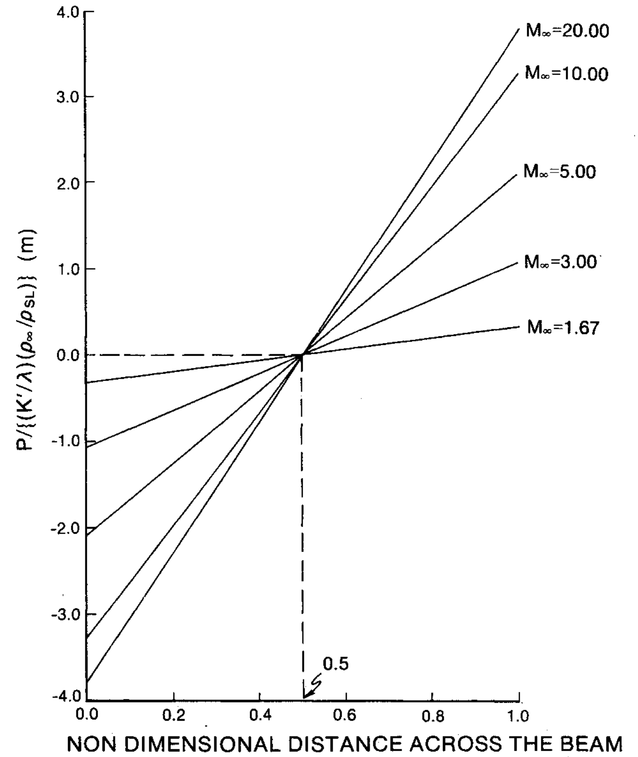

Fig. 12 Variation of P_{II}^{*} along a selected beam (evaluated at the receiving optics).

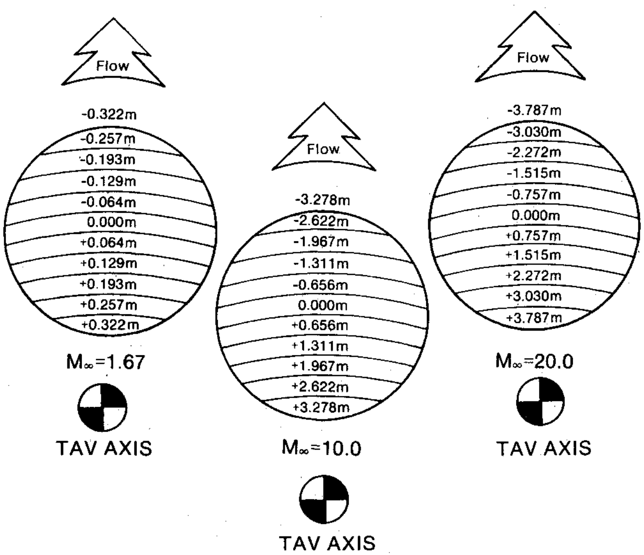

Fig. 13 Contours of constant P_{II}^{*} in the beam wave front located at the receiving optics. Three different Mach numbers are portrayed.

titude profile[3] given in Fig. 15. A mean value of the "optimized energy" and "optimized weight" trajectory-altitude profiles was used. The relationship between the Apollo Lightcraft altitude and the ratio ρ_∞/ρ_{SL} was derived from a standard atmosphere model.[14]

By using the above considerations and $D = 1.00$ m, $r_0 = 1.65$ m, $\kappa' = 2.3 \times 10^{-4}$, and $\lambda = 3.8$ μm, the maximum absolute value of the optical phase distortion (occurring at the studied wavefront) can be plotted against the flight Mach number in Fig. 16.

Figure 16 takes into account not only the altitude change, but also the change of propulsion modes. The discontinuity observed at Mach 10 represents the transition from the scramjet mode to the MHD-fanjet mode.

A major conclusion indicated in Fig. 16 is that the aero-optical phenomena will introduce considerable aberrations in the

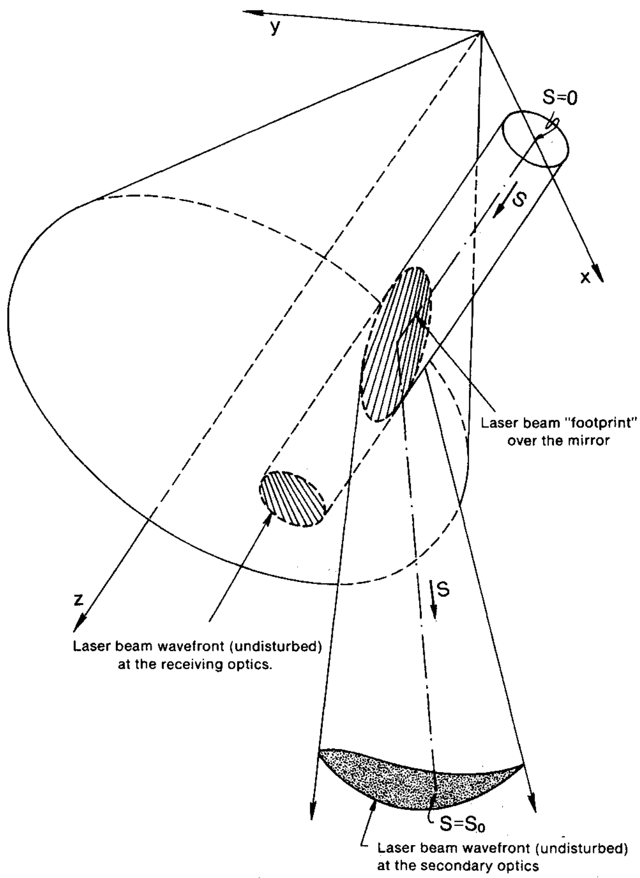

Fig. 14 Reflection of a cylindrical cross-section beam over an ideal mirror. The darkened surface represents the wave front after the conical reflection.

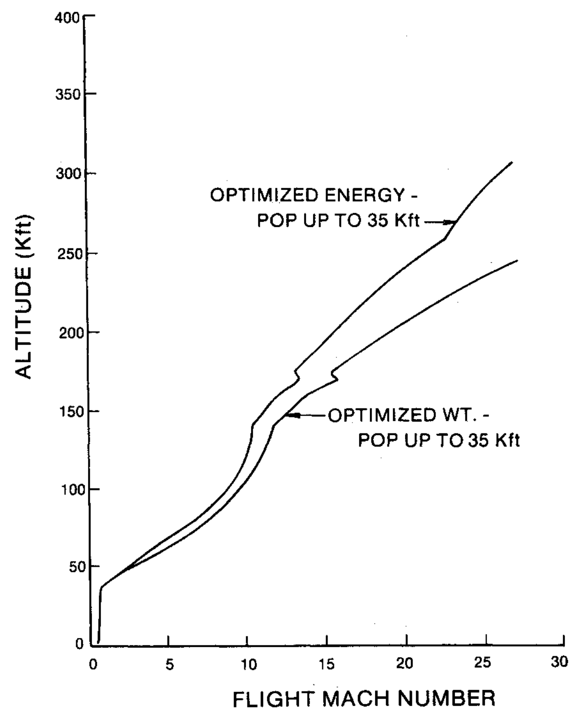

Fig. 15 Trajectory-altitude profile.

propulsive beam only during the beginning of the transatmospheric flight (i.e., at low altitudes). These aberrations can be obtained from the computed phase-distortion distribution and the Zernike polynomials,[4,5,7] which can then be delivered to an adaptive primary optics designed to partially overcome such

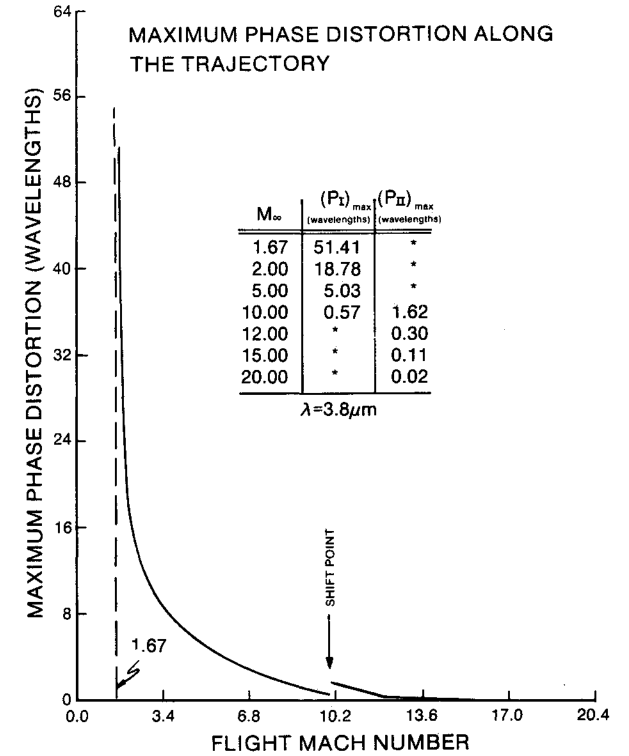

Fig. 16 Maximum phase distortion in the propulsive beam vs flight Mach number for a chosen trajector-altitude profile.

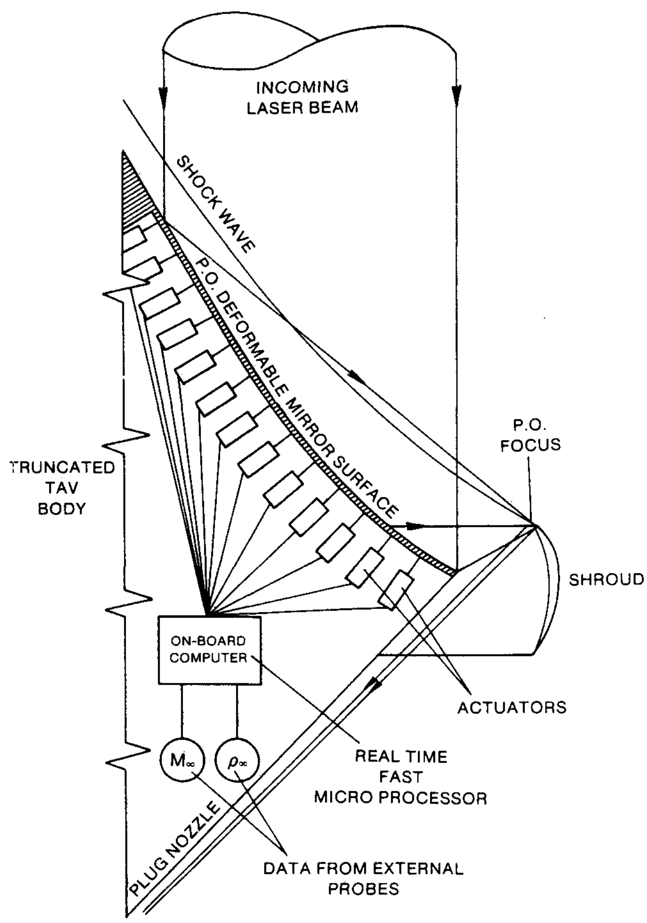

Fig. 17 Adaptive primary optics for the Apollo Lightcraft.

aberrations. Without complete wave-front correction at the primary optics, a considerable amount of laser power may be wasted. The entire purpose of this receptive optical train is to deliver laser-beam power into the working fluid of the combined cycle engine. The magnitude of phase distortions indicated in Fig. 16 leaves little doubt that the primary optics surface must be actively controlled.

Figure 17 portrays the concept of an adaptive primary optics for the Apollo Lightcraft. In this figure the actuators are shown underneath the mirror surface which would be controlled by an onboard high-speed computer. This computer would evaluate the intensity of the aberrations developed across the beam and then generate a counteraction by deforming the mirror surface. The entire system (computer and actuators) must respond quickly enough to accommodate the altitude and flight Mach numbers changes.

As a final remark, it is important to point out that although all of the phase-distortion calculations assumed a laser wavelength of 3.8 μm, phase distortions for different wavelengths can be readily scaled; as seen in Eq. (1), the wavelengh λ is only a dividing factor.

Conclusions

A very simple analysis of optical distortions in a propulsive laser beam due to a conical supersonic flowfield over a mirror/window was performed. From this analysis, one can expect considerable aberrations in a 3.8-μm propulsive laser beam during the low-altitude portion of a transatmospheric flight. As the TAV climbs to higher altitudes where the ambient density decreases, the optical phase distortion due to aero-optical phenomena is minimized.

Although the results indicate useful trends, the reader must keep in mind that the analysis ignores such important considerations as real-gas effects, actual Apollo forebody geometry, and viscous effects. These effects can possibly increase the predicted phase-distortion values, even in regions where it can now be neglected (e.g., during the MHD-fanjet mode).

By using Zernike polynomials, the intensity of the optical aberrations can be calculated; therefore a vehicle-based adaptive system can be designed to partially overcome the aberrations.

As a final conclusion, the present work attempts to give a rough prediction of the aero-optical phenomena to be expected during Apollo Lightcraft transatmospheric flights. Further investigations should be made in order to develop more realistic models for the aero-optical phenomena. Both theoretical and experimental investigations in this area will certainly open new perspectives for the "future of flight."

Acknowledgment

The authors wish to thank Henry T. Nagamatsu for his valuable advice and encouragement.

References

[1]Willinski, M. I., "Beamed Electromagnetic Power as a Propulsion Energy Source," *American Rocket Society Journal,* Vol. 29, Aug. 1958, pp. 601-603.

[2]Fisher, A., "Beam-Power Plane," *Popular Science,* Vol. 232, No. 1, Jan. 1988, pp. 62-65.

[3]Myrabo, L. N., et al., "Apollo Lightcraft Project," NASA/USRA Advanced Design Program, 3rd Annual Summer Conf., Washington, DC, June 1987.

[4]Fuhs, A. E., and Fuhs, S. E., "Optical Phase Distortion Due to Compressible Flow Over Laser Turrets," *Aero-Optical Phenomena,* edited by K.G. Gilbert and L.J. Otten, Vol. 80, Progress in Astronautics and Aeronautics, AIAA, New York, 1982, pp. 101-137.

[5]Born, M., and Wolf, E., *Principles of Optics*, Pergamon, New York 1964.

[6]Myrabo, L. N., "Advanced Energy Conversion Concept for Beamed-Energy Propulsion," Final Technical Rept., Air Force Office

of Scientific Research, AFOSR-84-0361, Aug. 1987.

[7]Hogge, C. C., Butts, R. R., "Frequency Spectra for the Geometric Representation of Wave-Front Distortions Due to Atmospheric Turbulence," *IEEE Transactions on Antennas and Propagation*, Vol. AP-24, 1976, pp. 144-154.

[8]Fuhs, A. E., "Potential Flow: Nonlinear Compressible Flow," Lecture 3B, Short Course on Laser Aerodynamics, Air Force Weapons Lab., Kirtland AFB, NM, April 11-22, 1977.

[9]Anderson, J. D., Jr., *Gasdynamic Lasers: A Introduction,* Academic, New York, 1976, Chaps. 10 and 11.

[10]Parmentier, E. M., and Greenbert, R. A., "Supersonic Flow Aerodynamic Windows for High-Power Lasers," *AIAA Journal,* Vol. 11, No. 7, 1973, p. 943.

[11]Liepman, H. W., and Roshko, A., *Elements of Gas Dynamics,* Wiley, 1957, Chap. 4.

[12]Kopal, Z., "Tables of Supersonic Flow Around Cones," Massachusetts Inst. of Technology, Dept. of Electrical Engineering, Cambridge, MA, 1947.

[13]Sims, J. L., "Tables of Supersonic Flow Around Right Circular Cones at Zero Angle of Attack," NASA SP-3004, 1963.

[14]U.S. Standard Atmosphere, U.S. Government Printing Office, Washington, DC, Dec. 1962.